AIAA JOURNAL
Vol. 44, No. 8, August 2006

Skin-Friction and Heat Flux Measurements in Shock/Boundary-Layer Interaction Flows

Erich Schülein*
DLR, German Aerospace Center, 37073 Göttingen, Germany

Modern nonintrusive techniques are used to make skin-friction and heat transfer measurements in two shock-wave/turbulent boundary-layer interactions (SWTBLIs). The two-dimensional SWTBLI is generated by impingement of an incident oblique shock wave on a flat-plate boundary layer. The three-dimensional SWTBLI results from the interaction of the swept shock generated by a fin with a flat-plate boundary layer. The measurements are made using the global interferometry skin-friction technique for the skin friction and the quantitative infrared thermography technique for the heat transfer rate. The results show that, for the two- and three-dimensional interactions, there is a clear difference in the behavior of skin friction and heat transfer as the strength of the shock is changed. This observation suggests that the analogy between momentum and heat transfer, which is the basis of many simplified physical models, is not valid in SWTBLIs. These new data supplement the previous measurements that include boundary-layer properties, surface pressure distributions, and patterns of the limiting streamlines. Taken together, these data complete a data set that is suited for computational fluid dynamics validation.

Nomenclature

A = amplitude of shock oscillations (computational fluid dynamics)
c_f = skin-friction coefficient based on incoming freestream conditions
c_m = specific heat capacity of model material
c_p = specific heat capacity of air at constant pressure
d_m = model wall thickness
h = oil film thickness or heat transfer coefficient
M, $\dot{m}$ = Mach number and mass flux
n = horizontal width, normal to limiting streamline (oil flow)
P_0, p = stagnation and static pressure
q, $\dot{q}$ = dynamic pressure and heat flux rate
R, R_1, R_2 = reattachment line, primary and secondary reattachment lines
Re_1 = unit Reynolds number
S, S_1, S_2 = separation line, primary and secondary separation lines
St = Stanton number
s = coordinate following limiting streamline
T_{IR}, T_R = temperature measured by infrared (IR) camera and background temperature
T_0, T = stagnation and static temperature
t, $t_{\min}$, $t_{\max}$ = time, lower and upper time limit (heat flux measurement technique)
U, U_{oil} = local flow velocity and averaged oil velocity
UI = upstream influence line
x, y, z = Cartesian coordinates
x_o, y_o, z_o = Cartesian coordinates with origin at model's leading edge
β = integral parameter in Eq. (7) and deflection angle of shock generator
δ, δ^*, θ = thickness, displacement thickness, and momentum thickness of boundary layer
ε = emissivity of model surface
λ, λ_m = optical wavelength and thermal conductivity of model material
μ = dynamic viscosity
ξ = inviscid shock strength
ρ, ρ_m = flow density and density of model material
σ = Stefan–Boltzmann constant
τ = shear stress

Subscripts and Superscripts

A = condition at cross-section A (Fig. 2a)
aw = adiabatic wall condition
e = condition outside boundary layer
m = model material condition
oil = oil condition
w = wall condition
0 = stagnation condition
0, 1, 2 = condition at different times
1, 2 = condition along primary (1) or secondary (2) separation or reattachment lines
∞ = freestream condition

Introduction

THE shock-wave/turbulent boundary-layer interactions (SWTBLIs) still belong to the fundamental problems of modern aerothermodynamics and high-speed fluid dynamics.[1,2] The importance of these phenomena stems not only from applied problems, such as the efficient design of control surfaces, high-speed inlets, or thermal protection systems, demanding safe prediction of surface heat and pressure loads, but also from purely fundamental interest in flows, which contain key problems of modern fluid dynamics: compressibility, turbulence, and viscous–inviscid interaction.

All modern numerical simulation methods, for example, Reynolds-averaged Navier–Stokes, direct numerical simulation, and large-eddy simulation, have difficulty in accurately prediction of flow properties in SWTBLI regions. The computed results show acceptable agreement with experimental data for the prediction of surface streamline pattern and pressure distributions, but significant disagreement, particularly in cases of strong shock-wave interactions, for skin friction and heat transfer data.[1] Therefore, in detailed experimental investigations of SWTBLIs, reliable skin-friction and heat flux measurements are especially valuable for

---

Presented as Paper 2004-2115 at the AIAA 24th Aerodynamic Measurement Technology and Ground Testing Conference, Portland, OR, 28 June–1 July 2004; received 14 December 2004; revision received 15 December 2005; accepted for publication 15 December 2005.

*Research Scientist, High Speed Configurations Division, Institute of Aerodynamics and Flow Technology; erich.schuelein@dlr.de. Member AIAA.

the validation of modern computational fluid dynamics (CFD) methods.

The inadequate knowledge about the true nature of the fluid dynamic phenomena plays a crucial role in flows with strong pressure gradients. The complex interaction of the momentum and heat transfer processes is understood (and can, therefore, be predicted) only for equilibrium flows. This also affects the quality of some indirect wall shear stress measurement techniques because the existing simplified physical models, applied for the calculation of the skin friction from the measured heat flux, are valid only for equilibrium or precalibrated flows. Therefore, the application of these models for flows with strong pressure gradients can lead to incorrect interpretations.[3] Direct and independent measurements of both heat transfer and skin friction in a variety of shock/boundary-layer interaction flows are necessary to improve the existing knowledge.

This paper presents results of experimental investigations of two CFD validation cases for SWTBLIs using modern nonintrusive methods for the measurement of skin friction and heat flux: two-dimensional oblique shock impingement on a flat plate and three-dimensional swept-shock interaction in the vicinity of a single-fin configuration. Both flows are relevant to supersonic inlet flows, where knowledge of the surface parameters in the interaction zone with high peaks in pressure, skin friction, and heat flux rates is at least as important as the downstream development of the flowfield parameters.

The incident shock wave interacting with the flat-plate turbulent boundary layer is a standard CFD validation case for two-dimensional SWTBLI (Refs. 1 and 4). It represents a simple test configuration for the validation of turbulence models and computational methods in predicting flow separation and recovery phenomena.[5–7] Because of technical problems with the realization of the two dimensionality of the flow in wind tunnels, only a few complete investigations exist that are considered suitable as CFD test cases. A detailed and recent review of several significant studies can be found in Ref. 1.

Three-dimensional interactions, which are more relevant for real applications, especially the swept- and crossing-shock interactions, have been studied to a great extent. Nevertheless, a recent review of the most significant experimental studies of three-dimensional SWTBLI (Ref. 1) has shown that too few validation data are available for three-dimensional interactions, especially with respect to complete experimental data sets of the most important flowfield and surface parameters. Moreover, there are still significant differences observed, for example, between the calculated and the experimental distribution of the skin-friction and the heat transfer coefficient in the interaction region.

The standard CFD validation case for a swept SWTBLI flow is the three-dimensional single-fin/flat-plate configuration.[1,2,8,9] The general property of the interaction flow is its quasi-conical nature. The structure of the swept SWTBLI footprint for fully developed separation flow, given in numerous papers, for example, Refs. 2, 8, and 10–12, is shown in Fig. 1. The designations in Fig. 1 are the upstream influence line (UI), primary and secondary convergence (or separation) lines S_1 and S_2, primary and secondary divergence (or reattachment) lines R_1 and R_2, the inviscid swept shock *Shock*, and the fin angle β. The virtual origin of the conical flow lies upstream of the fin's leading edge.[2,10] The structure of the flow depends most of all on the intensity of the swept shock. If the shock is strong enough, the flow separates from the surface and a quasi-conical vortex develops at the foot of the main swept shock.[10] The flow structure changes with increasing shock-wave intensity. Once a certain shock strength has been reached, a secondary separation appears in the flow underneath the main separation vortex. The limiting streamline pattern in Fig. 1 is typical for a very strong shock wave with fully developed flow structure. The existing descriptions of the flow topology comprise at least six different regimes in the development of the structure.[12] Details can also be found in the recent review in Ref. 1.

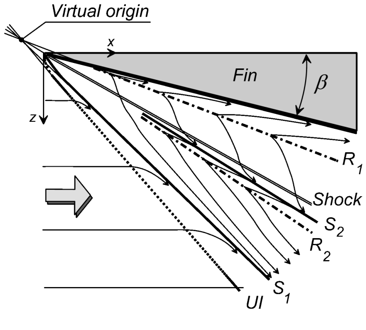

Fig. 1 Footprint of quasi-conical interaction flow.

The quasi-conical symmetry of the flow regarding the shock-wave structure, the surface pressure distribution, and the limiting streamline pattern is undisputed. However, it can generally not be expected that surface parameters, which are sensitive to the boundary-layer state, like skin friction and heat flux rate, will also remain constant along conical rays. To the author's knowledge, up to now this topic has not been explicitly addressed.

Recently, the first pointwise skin-friction measurements[8] in three-dimensional swept SWTBLI flows at Mach numbers $M_\infty = 3$ and 4 have shown, for example, that with increasing interaction strength, the relative peak of the skin-friction coefficient $c_{f\ \mathrm{peak}}/c_{f1}$ near the primary reattachment line R_1 grows progressively much faster than the shock strength itself. To answer the open questions about the development of skin friction at higher Mach numbers and shock strengths, as well as the behavior of the heat transfer peaks, is one of the objectives of this paper.

The goal of the present work is to enhance the existing data for several shock-wave/boundary-layer interaction cases by independently measuring heat transfer and skin friction, as well as to investigate the relations between momentum and heat transfer in interacting turbulent flows. The common analysis of the experimental surface pressure, heat transfer, and skin-friction distributions in each of these test cases should enhance the basic understanding of such flows.

Wind Tunnel and Flow Conditions

The present investigations were conducted in the DLR Göttingen Ludwieg Tube facility (RWG),[13] which covers a Mach number range of $3 \leq M_\infty \leq 7$ and a unit Reynolds number range of $5 \times 10^6 \geq Re_{1\infty} \geq 60 \times 10^6\ \mathrm{m}^{-1}$. Figure 2 shows the general arrangement of the wind tunnel; the main features and flow conditions for the two test tubes A and B are summarized in Table 1. A unique feature of the RWG is the use of a long tube as a pressure reservoir. The tube is closed at one end and has a gate valve attached to the other end; downstream of this are a supersonic nozzle, the test section, and the dump tank. After opening the gate valve, the flow is started by an expansion wave that travels to the closed end of the tube; the expansion wave is reflected at the closed end and travels back downstream. As long as the expansion wave does not return to the nozzle throat, the test gas flows, at constant stagnation conditions, through the nozzle and test section into the dump tank. The tube length of 80 m results in a run time of about 0.3 s. The test section for the Mach numbers $M_\infty = 3$–4 (tube A) has a cross section of $0.5 \times 0.5\ \mathrm{m}^2$, whereas for the high Mach numbers (tube B) the circular section has a diameter of 0.5 m. The low costs of operation, a relatively large test section, and good optical access make this facility well suited for optical experimental methods such as the oil-film interferometry technique.

The nominal freestream conditions in the test section for the present investigations are Mach number $M_\infty = 5$, total temperature $T_0 = 410$ K, and total pressure $P_0 = 2.12$ MPa (which correspond to a unit Reynolds number of about $Re_{1\infty} = 37 \times 10^6$/m). The run-to-run variations in the local freestream Mach number M_e and velocity U_e are less than 0.5% and within 2% for the static temperature T_e. The wall temperature of the test model during the run is mostly 300 ± 5 K, with exception of the heat flux measurement tests. The special model inserts used in these tests, which are fabricated from a material with a low thermal conductivity, show a noticeable adiabatic heating.

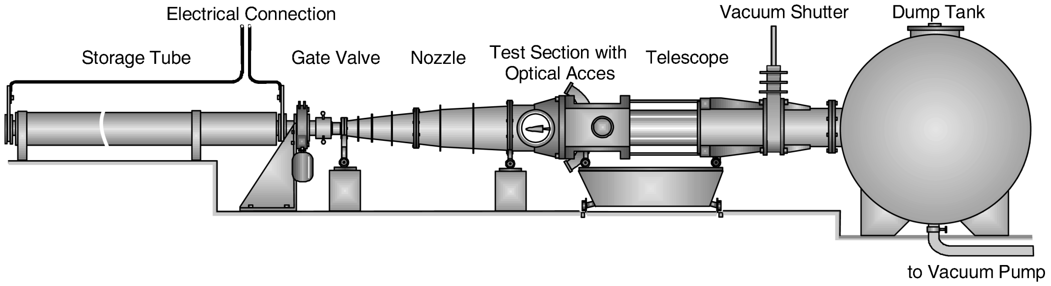

Fig. 2 Super- and hypersonic RWG.

Table 1 RWG main features and flow conditions

Performance	Tube A	Tube B
Maximum stagnation pressure, bar	15	40
Maximum stagnation temperature, °C	20	400
Mach number	2.79–4.65	5.0–6.9
Unit Reynolds number, 10^6 m^{-1}	5–60	5–50
Run time, s	0.4	0.3
Test section	0.5×0.5 m^2	ϕ 0.5 m

Measurement Techniques and Instrumentation

Optical Skin-Friction Measurements

The difficulties of direct shear stress measurements in interacting flows or in flows with thin boundary layers are well known.[3,14] They are mainly related to the intrusiveness of the measuring device and the corresponding flow disturbance. The oil-film interferometry technique overcomes many of these limitations because it provides nonintrusive measurements. The technique is based on the relationship between the local surface shear and the thinning of an oil film, placed on the test surface and exposed to the flow (Fig. 3a). The rate of thinning of the oil film is determined from the optical interference that is created when an incident light beam is partially reflected off of the oil and test surfaces (Fig. 3b). This technique, originally used in low-speed flows,[15] has been extensively modified in recent years for use in high-speed three-dimensional flows and is commonly referred to as the global interferometry skin-friction (GISF) technique. Modern GISF methods for three-dimensional gradient flows can be divided into two categories: 1) one-image methods, which require only one interferogram and knowledge of the total run time t for the calculation of the skin friction, and 2) two-image methods, where at least two images and the corresponding time interval Δt have to be obtained during the run. A recent review of different GISF approaches can be found in Ref. 14. Generally, the one-image methods are simpler, but the precise requirement of the total run time can lead to measurement errors, especially in short-duration wind tunnels. Because both one- and two-image methods are based on the same general thin-oil-film equation,[14] the different relations that are used for the skin-friction calculation in each case can be converted into each other, assuming equivalent run time and a constant local wall shear stress over time.[16] The performance of the known GISF methods under the specific conditions of a short duration wind tunnel has been analytically investigated using different two-dimensional and three-dimensional flows having given shear-stress distributions. The analytical results show good agreement with the specified distributions and confirm the reliability of these methods.[16] The choice of which method to use in a wind tunnel test is, however, often based on more practical constraints of the wind-tunnel facility.

In the present work, the two-image method[17,18] is used to determine skin friction. The local wall shear stress τ_w at a given position is determined from the measured evolution of the oil-film thickness h over the time duration t. The oil viscosity μ_{oil} and horizontal width of the oil stream n for each streamline coordinate s (Fig. 3a) are known or measured quantities. This technique is based on a version of the thin-oil-film equation that is generalized for two-dimensional oil flow; the basic steps of this generalization are summarized here, but more complete details can be found in Ref. 17. The mass flux of the elementary oil stream across the cross section A at the distance s_A from the oil-film leading edge (Fig. 3a) can be determined either from the oil velocity $U_{\text{oil}A}$ averaged across the area A

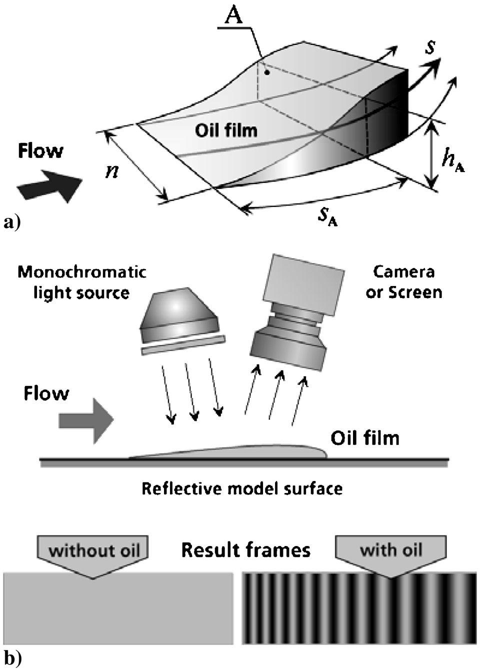

Fig. 3 Principle of oil-film interferometry.

$$\dot{m}_A = n_A h_A \, \rho_{\text{oil}} U_{\text{oil}A} \tag{1}$$

or, alternatively, from the diminution of the total amount of oil above the area given by the length s_A and the width n

$$\dot{m}_A = \rho_{\text{oil}} \frac{\mathrm{d}}{\mathrm{d}t} \int_0^{s_A} nh \, \mathrm{d}s \tag{2}$$

Because the flow in the thin oil film can be described as a Couette-flow, that is, the viscous layer flow between two flat surfaces that slide parallel to each other, the local oil velocity distribution is given as[19] $u(y) = \tau_w y/\mu$ and the average oil velocity $U_{\text{oil}A}$ for the layer of thickness h is then given as $U_{\text{oil}A} = \tau_w h/(2\mu_{\text{oil}})$. Combining Eqs. (1) and (2) with this relation for $U_{\text{oil}A}$ yields the equation for the wall shear stress at the coordinate s_A (Refs. 17 and 18),

$$\tau_w = \frac{2\mu_{\text{oil}}}{n_A h_A^2} \frac{\mathrm{d}}{\mathrm{d}t} \int_0^{s_A} nh \, \mathrm{d}s \tag{3}$$

The experimental setup used in the RWG is shown schematically in Fig. 3b. The light source is a low-pressure sodium vapor lamp with an opal diffusing element between the light source and the model surface. To improve the reflection properties, a dark self-adhesive polyethylene foil is attached to the model surface. Because of the very short test time in the facility, the interferograms are recorded as a sequence of 8-bit gray-scale single images (1024 × 1024) during a run using an ADIMEC® 12XP charge-coupled device camera at a rate of 30 frames/s; the images are stored on a personal computer's hard disk. Because of the time required for the development of the thin oil film on the test surface at the beginning of a run, only from four to six frames can be used for the skin-friction calculation using the GISF technique. The best results are obtained with the WACKER® AK-10 silicon oil, which has a nominal viscosity of 10 mm^2/s (=10 cSt) at 25°C. A similar liquid mixture of this oil with TiO_2-powder is used for the surface flow pattern visualization. The movement of the particles in the mixture along the limiting streamlines is recorded using the equipment just described and is used to determine the direction of the limiting streamlines.

The measurement uncertainties of this GISF technique in the short-duration facility RWG are, in general, larger than in conventional blowdown wind tunnels. The largest uncertainty arises from the needed to use oil with a very low viscosity because of the very short run time. On the other hand, there are also positive aspects of this short test time because the good thermal conductivity of the steel model renders the temperature sensitivity of the oil viscosity not a major issue. The model wall temperature is measured in separate runs using an infrared (IR) camera, and these measured data are used for the temperature correction of the viscosity. In general, the repeatability error in the skin friction varies from ±4% in undisturbed boundary layers up to ±10% at the highest wall shear-stress levels near the reattachment lines. The uncertainty within a single run for the analysis of the obtained skin-friction distributions is substantially smaller.

For image acquisition, image processing, and skin-friction computations, a software application developed in earlier works[16,20] is used. More details about the GISF technique and its application for measurements in short-duration facilities can also be found in Ref. 21.

Heat Flux Measurements

Two different transient techniques are used for the heat transfer measurements in the RWG: the thin-skin and the thick-wall techniques.

The thin-skin technique can be applied if the wall temperature normal to the model surface can be assumed uniform and the lateral heat conduction in the wall can be neglected. These conditions are attained if the thin-wall test model is manufactured from materials such as copper, nickel, etc., that have a high thermal conductivity, and if the heat transfer between the flow and model wall starts rapidly, such as in a short-duration wind tunnel. This heat transfer measurement technique was the preferred method in earlier investigations conducted in the RWG[5] and is used in the two-dimensional SWTBLI studied in the present investigation. The local heat flux rate $\dot{q}$ is directly calculated from the measured rise of the wall temperature T_w,

$$\dot{q} = \rho_m c_m d_m \frac{\mathrm{d}T_w}{\mathrm{d}t} \tag{4}$$

for $t_{\min} < t < t_{\max}$. The most accurate way to determine the limiting values $t_{\min}$ and $t_{\max}$ is from observation of the slope of the wall temperature during the tunnel run because valid results are only obtained when $\mathrm{d}T_w/\mathrm{d}t$ is constant. For the thin-skin nickel model used in the present investigations, which has material properties of $\rho_m = 8900$ kg/m^3, $c_m = 458$ Ws/(kgK), and a wall thickness of $d_m = 0.2$ mm, $t_{\min}$ is of the order of 1 ms and $t_{\max}$ is slightly less than 130 ms.

The thick-wall technique is applied to a solid- or thick-walled model that is fabricated from a material with low thermal conductivity λ_m. The time history of the surface temperature is recorded during the wind-tunnel run and is then used to determine the heat transfer rate under the assumption of a semi-infinite wall thickness. For a semi-infinite slab that is exposed rapidly to a constant heat flux rate $\dot{q}$ at time t_0, the solution of Fourier's partial differential equation is [22]

$$\dot{q} = \sqrt{\frac{\pi \rho_m c_m \lambda_m}{4(t - t_0)}}(T_w - T_{w0}) \tag{5}$$

T_w and T_{w0} are the current and initial surface temperatures. Because the exact run time in short-duration facilities is mostly unknown, but at least two values of the wall temperature T_{w1} and T_{w2} at different times t_1 and t_2 are available, in the present work Eq. (5) is rewritten for constant heat transfer rates

$$\dot{q} = \sqrt{\frac{\pi \rho_m c_m \lambda_m}{4(t_2 - t_1)}(T_{w2} - T_{w1})(T_{w1} + T_{w2} - 2T_{w0})} \tag{6}$$

In the case where there is a significant surface temperature rise compared to the adiabatic wall temperature T_{aw}, the heat transfer solutions for constant heat transfer rates are not applicable. In this case, with variable heat flux rates, Eq. (5) is replaced by[22]

$$(T_w - T_{w0})/(T_{aw} - T_{w0}) = 1 - e^{\beta^2}\operatorname{erfc}(\beta)$$

$$\text{for} \qquad \beta = [\dot{q}/(T_{aw} - T_w)]\sqrt{(t - t_0)/(\rho_m c_m \lambda_m)} \tag{7}$$

In the present application, the surface temperature of the test model insert, which is made from black Plexiglas®, is measured by a high-speed IR camera system FLIR ThermaCAM® SC500. When it is combined with a high-speed digital recording and temperature analysis system, the IR camera offers high performance for applications in short-duration facilities. This real time IR camera system allows the storage of a sequence of 14-bit single noninterlaced images (240 × 320) at rates up to 50 frames/s. The IR camera is based on a focal-plane array that is sensitive in the spectral range from 7.5 to 13 μm. The manufacturer's quoted accuracy is of the order of ±2% (maximum ±2°C) in the entire measurement range from −40 to 120°C (or from 0°C to 500°C), and the thermal resolution is of the order of 0.07°C at 30°C.

Optical access to the test section in the RWG is provided through a custom-built antireflection-coated germanium window. The entire measurement setup is calibrated using a precision blackbody heat emitter that is positioned in the test section; this yields the actual transmission coefficients of the IR window. The surface emissivity ε of the model material is measured indirectly by assuming that $\varepsilon = 1 -$ (reflectivity). In this case, the relation between the actual wall temperature T_w and the wall temperature that is measured by the IR camera T_{IR} at the background temperature T_R is given by the Stefan–Boltzmann law as

$$\sigma T_{\mathrm{IR}}^4 = \varepsilon \sigma T_w^4 + (1 - \varepsilon)\sigma T_R^4 \tag{8}$$

The surface emissivity ε is obtained in pretest calibrations at known temperatures T_w and different background temperatures T_R that are realized by use of the precision blackbody heat emitter.

In the present application, the resulting image size for a typical object placed at 0.3 m in the test section of the RWG is approximately 94 × 125 mm^2. This corresponds to a spatial resolution on the model surface of about 0.4 mm or to a pixel size of 0.16 mm^2. The high number of measurement points (76,800 pixels) and good spatial resolution make this measurement technique superior to conventional thermocouple-based techniques.

The experimental local heat flux rates $\dot{q}$ obtained in the present work are nondimensionalized with respect to freestream conditions:

$$St = \dot{q}/\rho_\infty U_\infty c_p (T_0 - T_w) \tag{9}$$

Extensive tests in the RWG show that, for high heat flux rates up to about 200 kW/m^2, the quantitative IR thermography technique yields good results that compare well with the more widely used thermocouple-based thin-skin technique. In the worst case, the repeatability error is ±5%. Thus, the temporal resolution and measurement accuracy of the IR-camera system are sufficient for the present experiments.

Results and Discussion

Two-Dimensional Incident Shock/Turbulent Boundary-Layer Interaction at Mach 5

The test model used for the investigations of the incident shock wave interacting with the flat-plate turbulent boundary layer is shown in Fig. 4. The flat plate, on which the boundary layer develops, has a sharp leading edge (thickness of approximately 0.1 mm) and is 500 mm in length and 400 mm in width. The shock generator plate (300 mm in length and 400 mm in width), which can be mounted with deflection angles β of 6, 10, and 14 deg, is positioned above the main plate so that the inviscid shock impingement position is 350 mm from the leading edge of the lower plate. The natural transition on the main plate, at the indicated freestream conditions is at $x_o = 120$ mm; thus, at the impingement position, the boundary layer is turbulent and well developed. At $x_o = 336$ mm the thickness of the boundary layer is $\delta = 4.7$ mm, the displacement thickness $\delta^* = 1.9$ mm, and the momentum thickness $\theta = 0.19$ mm. The incoming flow conditions as well as the main experimental data are described in detail in Refs. 4 and 5.

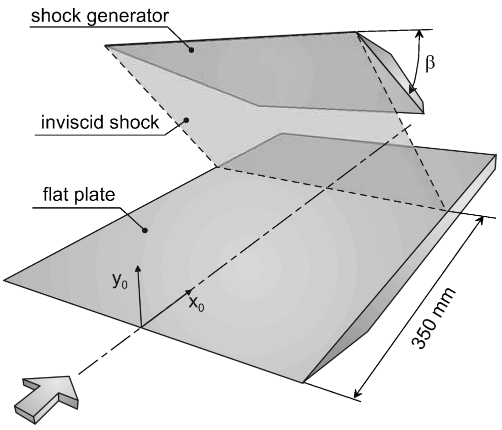

Fig. 4 Test model.

The flow cases obtained with the three different shock generator angles β result in different degrees of flow separation, including the weak interaction case (6-deg generator angle) without separation, the medium interaction case (10 deg) with a small separation zone, and the strongest (14-deg) interaction case with a significant separation. The experimental data, shown in Fig. 5, include spark shadowgrams and quantitative flowfield diagrams.[4] The numbered arrows at the bottom of each flowfield diagram show the positions of the measured pitot and static pressure surveys, which are used for the determination of the boundary-layer properties. The position of the flow separation S and reattachment R points for $\beta = 10$ and 14 deg are marked by black arrows. The outer edge of the boundary layer, as well as the positions of the shock waves and the contours of expansion fans, is determined from resulting flowfield profiles and shadowgrams. The relatively large dimensions of the model results in a large region downstream of the shock/boundary-layer interaction, within which the evolution of the disturbed boundary layer may be investigated in the absence of additional pressure gradients or noticeable three-dimensional effects.

The measured skin-friction and Stanton number distributions are compared to the wall pressures for the $\beta = 10$ and 14 deg cases in Fig. 6. The flowfield diagrams (Fig. 5, right) and the wall pressure distributions (Fig. 6a) show that the distance between the shock impingement position and the incidence of the first characteristic of the expansion fan, which emanates from the trailing edge of the shock generator, decreases with increasing deflection angle; however, this distance is always greater than 90 mm ($>20\,\delta_1$).

The surface distributions show that the extent of the separation zone increases as the shock generator angle β is increased from 10 to 14 deg (Fig. 6). Negative skin-friction values in the interaction region, measured with the GISF technique, indicate a region of flow reversal even in the case of the small separation zone for $\beta = 10$ deg.

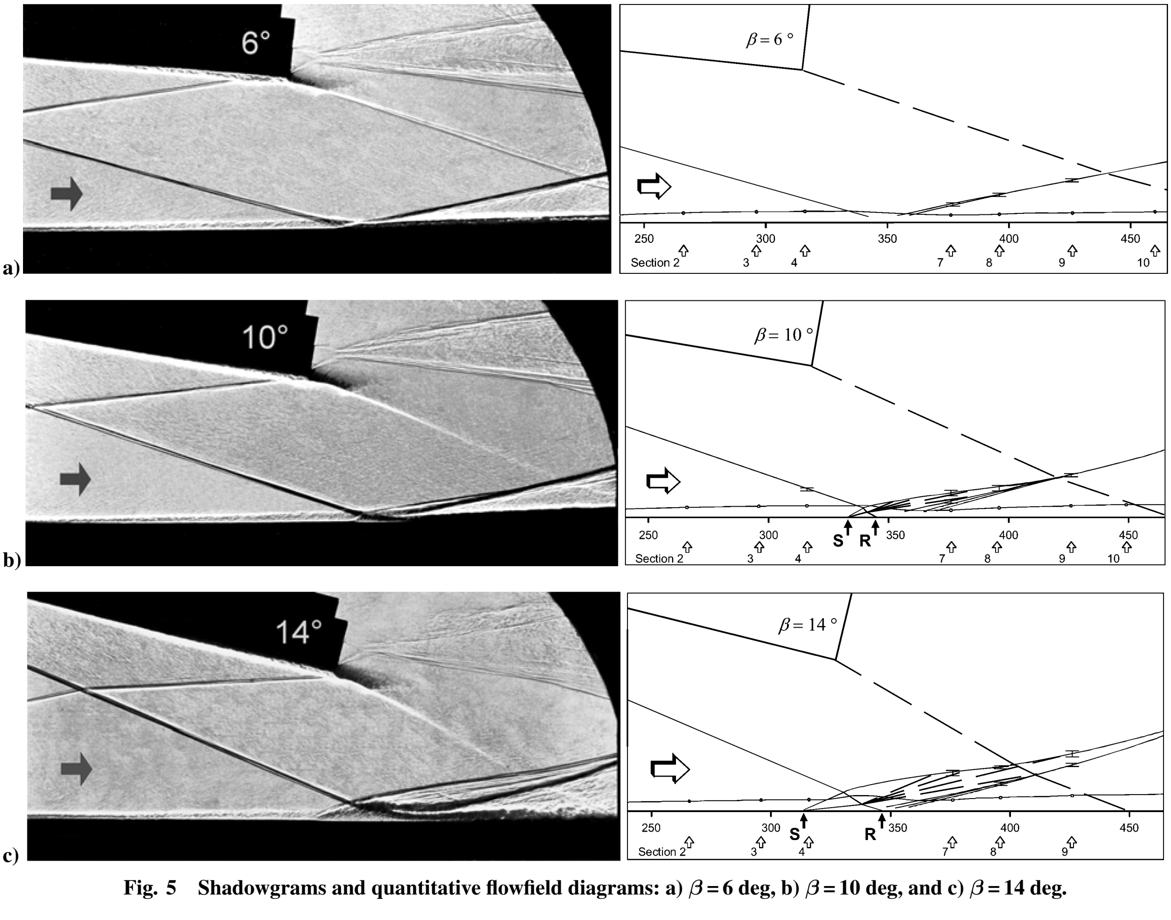

Fig. 5 Shadowgrams and quantitative flowfield diagrams: a) $\beta = 6$ deg, b) $\beta = 10$ deg, and c) $\beta = 14$ deg.

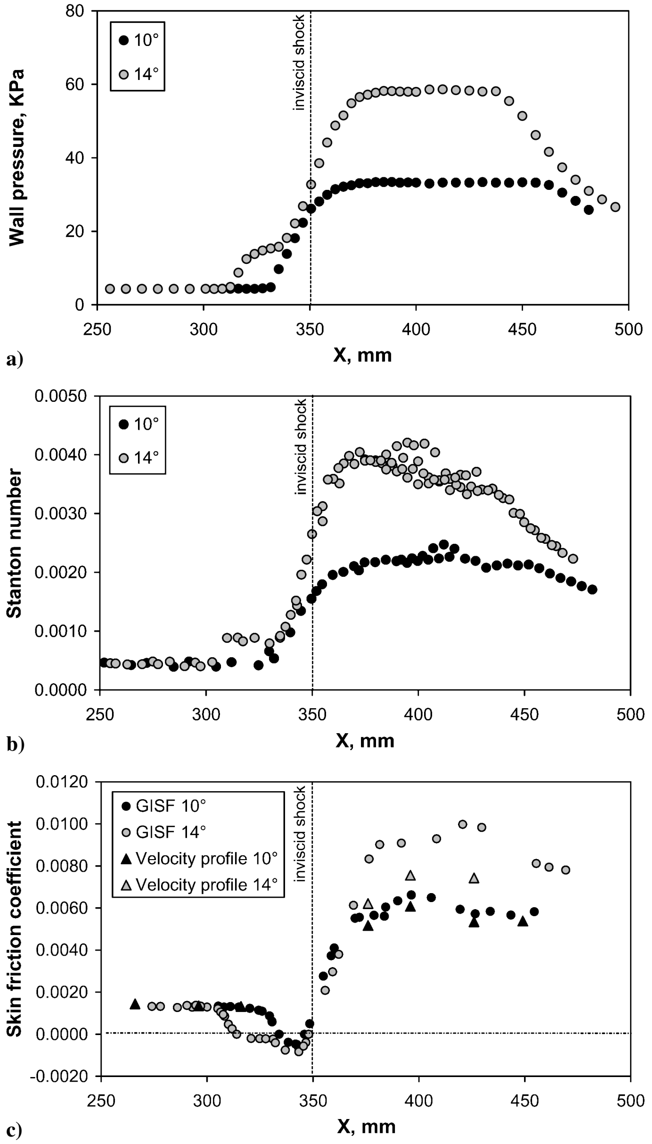

Fig. 6 Surface properties for $\beta = 10$ and 14 deg cases: a) wall pressure, b) Stanton number, and c) skin-friction coefficient.

Of course, the zero values of the skin friction at the separation and reattachment points cannot be measured by GISF; they are estimated from conventional oil-flow visualization.

In the separation zone, a very remarkable effect is observed. Although, as expected, the skin friction decreases in the vicinity of the separation point, the heat flux increases in the separation zone. This effect is more pronounced for the $\beta = 14$ deg case, but is also noticeable for the $\beta = 10$ deg case. This is indicative of the complex nonequilibrium behavior in these turbulent interacting flows, in which the Reynolds analogy between momentum and heat transfer is not valid. In regions with strong SWTBLI this is expected. Therefore, the results of the detailed quantitative analysis[7] of Reynolds analogy principles on the basis of present experimental heat flux and skin-friction data show its good correlations only outside of the interaction region, for an undisturbed boundary layer and downstream of the heat flux peaks behind the interaction.

The opposite trends in the distributions of heat transfer and wall shear stress mean that the heat transfer elevated near the separation S and reattachment R points, whereas the skin friction is zero. Such an increase in the heat flux rate in a separated flow region is also observed in other studies of two-dimensional interactions,[1] and this phenomenon is a common feature of turbulent flows. Previous studies of laminar boundary layers, for example, Ref. 23, however, do not show this phenomenon. That is, the heat transfer rates in laminar separation flows decrease in manner similar to the wall shear stress. The amplification of turbulence in the boundary layer and in the external flow due to the interactions with the shock waves,[1] as well as the higher surface pressure and density due to the stronger separation shock (compared to similar interactions in laminar flows) are possible explanations for the observed increase in the surface heat transfer in the interaction region.

The increase of heat flux downstream of the reattachment to levels that are higher than in the undisturbed flow occurs at a similar location to that seen in the surface pressure and wall shear stress distributions. In addition to the amplification of turbulence energy, discussed earlier, the increase in the local dynamic pressure downstream of the shock interaction and the development of a new boundary layer in the wall region of the attaching flow[1] are possible reasons for this behavior.

The locations of the peaks in the Stanton number and the skin friction indicate approximately the end of the recompression region downstream of the shock reflection. Although the development of the flow downstream of this region occurs in the absence of pressure gradients, an equilibrium state is not reached within the region of measurements. This observation is also seen in the measured boundary-layer profiles that are reported in Ref. 4. Furthermore, a comparison of the experimental skin-friction distributions (Fig. 6c), derived from the GISF technique, to the distributions obtained from the velocity profile technique,[4] also show this. Specifically, in the undisturbed boundary layer upstream of the interaction, the two measurements are in very good agreement. However, downstream of the interaction zone, in particular for the strongest interaction case, $\beta = 14$ deg, there are some significant differences between the two measurements. The comparisons show that there are limits in the use of the velocity profile technique because the technique is based on the assumption of a turbulent logarithmic law for the velocity profile. This technique will, therefore, not yield accurate results in regions with nonequilibrium boundary layers. The GISF technique does not have these limitations and, thus, yields more reliable results.

The present experimental data have been used for validation purposes in several numerical investigations.[5–7] Fedorova and Fedorchenko[5] have solved the unsteady two-dimensional Favre-averaged Navier–Stokes equations in strong conservation form using the Wilcox k–ω turbulence model. The comparison of experimental and computed profiles of mean velocity, density, and temperature, and the distributions of surface pressure, skin friction, and heat flux, show different levels of agreement. The computed wall pressure distributions agree well with experimental results for the three test cases. The skin-friction distributions are well predicted except in the strongest interaction case, where the level of skin friction downstream of the interaction is underpredicted. The comparison of the experimental and computed Stanton numbers shows further differences. For the weakest interaction case, $\beta = 6$ deg, the computed results are in good agreement with the experiment, whereas for the cases with flow separation, $\beta = 10$ and 14 deg, the computations overpredict the heat transfer just downstream of the reattachment. Farther downstream, the computed heat transfer decreases to the levels measured in the experiment. Further computations[24] have been conducted to determine the possible reasons for the discrepancies in the strongest interaction case. These computations include a model to account for the unsteadiness of the incident shock. The results of these calculations (Fig. 7; $\beta = 14$ deg), with a frequency of shock-wave oscillations of 1 kHz, show that, at a sufficient amplitude A, the calculated distributions are closer to the experimental data, and the heat flux does not overshoot the measured data. It is generally accepted that the unsteadiness of the shock system in turbulent separated flows is a consequence of the shock-wave interaction with the large eddies in the incoming boundary layer. The computed results show that there may be a significant influence of the unsteadiness of the shock system on the heat flux distribution.

Steelant[7] has used the present experimental data to examine the effects of a compressibility correction in turbulence models. The results show that, for the test cases, there is good agreement between the computation and experiment for most of the surface parameters

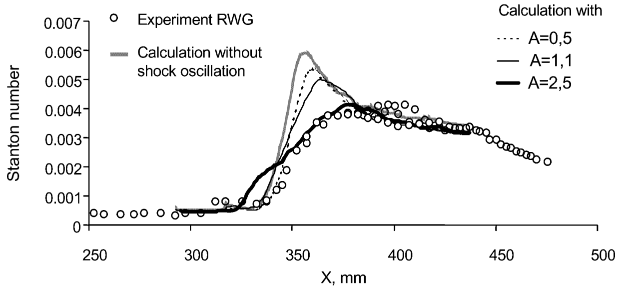

Fig. 7 Shock oscillation influence on Stanton distribution, oscillation frequency 1 kHz (Ref. 24).

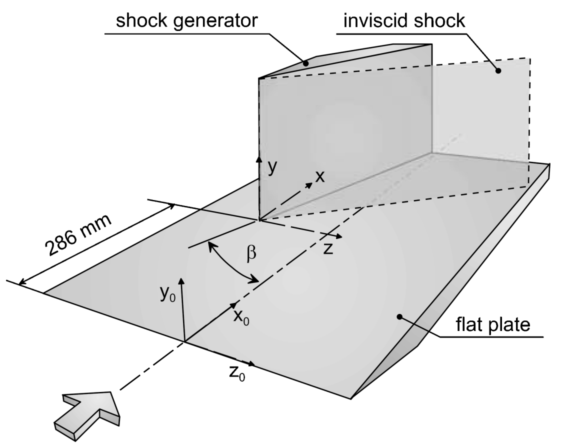

Fig. 8 Test model.

outside of the separation region. However, in the vicinity of the separation bubble the agreement is not as good. As in the computations discussed earlier,[5,24] the surface pressure and the skin-friction distributions show better agreement than the heat transfer. It is evident that the prediction of the heat transfer is still the most challenging aspect of these flows, particularly in the region of the recirculation bubble.

These discrepancies between the experimental and computed heat transfer rates are larger than the measurement uncertainty of ±5%. This suggests that the measurements are not the source of errors, but rather that the problem is in the prediction of the heat transfer. In the computation, both the inability of the turbulence model to describe correctly the development of turbulence intensity in disturbed boundary layers downstream of the SWTBLI and that the computational models do not include effects such as an increase of turbulence energy by the acoustic waves coming from the boundary layer developing on the surface of the shock generator are possible sources of error.[5]

Three-Dimensional Swept SWTBLI Flow

The configuration used for the investigations of three-dimensional swept shock-wave/boundary-layer interaction flows is shown in Fig. 8. It consists of an unswept sharp fin that acts as the shock generator, mounted on a flat plate. The fin may be mounted at different deflection angles β in the range from 2 to 27 deg. The flat plate has a sharp leading edge and is 500 mm in length and 400 mm in width. The fin has a height of 100 mm and a length of 260 mm. The distance between the leading edges of the flat plate and of the fin is 286 mm at $\beta = 23$ deg. The natural transition on the flat plate occurs at approximately $x_o = 120$ mm, and at the position of the fin's leading edge the boundary layer is turbulent. At $x_o = 266$ mm the thickness of the boundary layer is $\delta = 3.8$ mm, the displacement thickness $\delta^* = 1.6$ mm, and the momentum thickness $\theta = 0.16$ mm. More details about the model geometry and flow parameters can be found in Ref. 25.

In a previous study,[25] three-dimensional swept and crossing-shock/boundary-layer interaction flows have been examined. The data obtained in this study include surface flow pattern visualizations and measurements of surface pressure and heat flux. The deflection angles of the single fin are from 2 to 27 deg for the swept SWTBLI (Fig. 8) and from 8 to 23 deg for the crossing SWTBLI in the double-fin configuration. Analysis of the angles of the separation and reattachment lines shows good agreement with empirical correlations, which were developed for lower Mach number (from two to four) flows.[12] These data have subsequently been used for CFD code validation, such as described in Ref. 9.

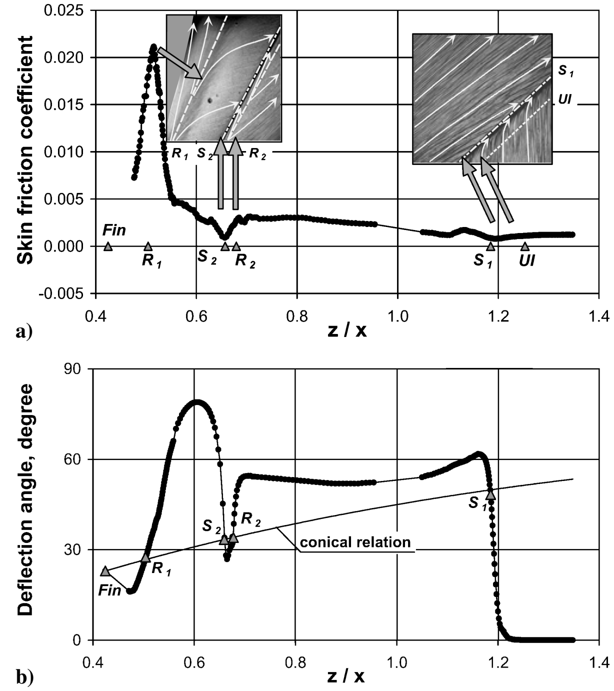

Fig. 9 Results for 23-deg single fin at $x = 122$ mm: a) skin-friction coefficient and b) direction of limiting streamlines.

The present experiments supplement these data with optical skin-friction measurements obtained by the GISF method and IR heat flux measurements. These new measurements on the single fin on the flat plate include skin-friction measurements for the fin angle of 23 deg and heat flux measurements for the angles of $\beta = 8$, 12, 18, and 23 deg.

Figure 9 shows the distributions of the skin-friction coefficient and the deflection angle of the limiting streamlines. The location of the measurement plane is $x = 122$ mm (where x is measured downstream from the fin's leading edge along the streamwise coordinate). The data are presented with respect to the conical coordinate z/x.

The distribution of the skin friction shows that there are higher levels of shear stress along the reattachment lines and lower levels along the separation lines. In contrast to two-dimensional flows, the skin friction at the separation lines is not zero because there is flow along these swept lines. The locations of the separation and reattachment lines are indicated in Fig. 9. These locations are seen to coincide with peaks and valleys in the measurements of skin friction. Between the upstream influence line (UI) and the primary separation line S_1, the skin-friction coefficient decreases as is expected for a separated three-dimensional flow. The impingement of flow along the reattachment line R_1 results in the relatively high wall shear stress.[8,10] This shear stress decreases toward the secondary separation line S_2 where its magnitude is close to that along the primary separation line S_1. A second peak in the skin friction is seen along the secondary reattachment line R_2. The skin-friction measurements in the vicinity of the secondary flow separation are well resolved, which is indicative of the good sensitivity of the GISF technique. Finally, in the region between the secondary reattachment line R_2 and the primary separation line S_1 there is a small decrease in the wall shear stress.

These observations are in good qualitative agreement with the point oil interferometry measurements reported in Ref. 8 for lower

Mach numbers and weaker shock strengths. However, the present measurements and the results from Ref. 8 differ in two respects. First, in Ref. 8 it is found that the location of the primary peak in the skin friction c_f differs by about 3 deg from the location of the primary reattachment line R_1. On the other hand, the present results show that these two locations are coincident (Fig. 9a). A second difference is that in Ref. 8 a local peak in the skin friction is measured intermediate to the UI and the primary separation line S_1. In the present work, this peak is located close to the primary separation line S_1 (Fig. 9a) within the separated flow region. As is discussed later, within the separated flow, there is also a peak in the measured heat transfer rates. This peak arises because the reversed flow accelerates toward the primary separation line S_1 due to the presence of a favorable pressure gradient.

In spite of these differences, the present work identifies a peak in the skin friction near the secondary separation line S_2; this feature was first described in Ref. 8. In the present work, this peak is thought to arise due to the flow impingement along the secondary reattachment line R_2 (Fig. 9), in a manner similar to that described for primary reattachment line R_1.

Figure 9b shows the measured angles of the directions of the limiting streamlines (also termed skin-friction lines). The line of the function arctan (z/x), which represents the relation for the ideal conical flow symmetry (conical relation), is also shown here. It is evident that only the separation lines S_1 and S_2 and reattachment lines R_1 and R_2 satisfy the conical relation. This indicates that the quasi-conical shock-wave structure determines these features in the flow.[10] There is a small difference between the measured and calculated angles at these four locations, and this is thought to occur because the virtual origin of the quasi-conical flow is upstream of the fin's leading edge (Fig. 1).

Several features of the distribution of the angles of the limiting streamlines are noteworthy. First, the largest angle lies between the primary reattachment and secondary separation lines, R_1 and S_2, respectively (Fig. 9b). Second, there is a nearly constant angle between the reattachment and separation lines R_2 and S_1, as can be seen from the plateau in the distribution between these locations. Third, there is a local peak just downstream of the separation line S_1; this peak arises due to the suction of the flow in the region of a favorable pressure gradient, as described earlier.

The distributions of surface pressure, heat transfer, and skin friction at several measurement planes are shown in Fig. 10. The relatively large distance between the most upstream ($x = 82$ mm) and downstream ($x = 182$ mm) planes is $\sim 25\delta$. Thus, the character of the boundary layer changes noticeably between these two planes. This can be seen in the different trends in the heat transfer distributions over the region where the surface pressure is approximately constant between the secondary reattachment R_2 and primary separation S_1 lines. The surface pressure distribution, which is largely determined by the quasi-conical nature of the shock-wave structure, changes little at all measurement planes (Fig. 10a). The distribution of skin friction is little changed at the different measurement planes (Fig. 10b), whereas the heat transfer rates decrease noticeably farther downstream of the leading edge (Fig. 10c).

These results confirm that the state of the boundary layer has a larger effect on the heat transfer processes than on the skin friction.

Also note that the maxima in the surface pressure, skin friction, and Stanton number are located along the primary reattachment line R_1 in all measurement planes (Fig. 10). Only at the most downstream measurement plane ($x = 182$ mm) are the peaks in St and c_f lower than expected. It is thought that the relative short fin (height of 100 mm) results in a tip leakage flow that reduces the skin friction and heat flux peaks at this most downstream location; the pressure is apparently less sensitive to this process.

The results of the three-dimensional SWTBLI are summarized by examining the effect of the shock strength on the peak values of the measured parameters. The peak values (excluding those measured at $x = 182$ mm) are normalized by the undisturbed values measured upstream of the interaction region at $z/x \approx 1.3$. These normalized parameters, wall pressure $p_{w\,\mathrm{peak}}/p_{w1}$, skin-friction coefficient $c_{f\,\mathrm{peak}}/c_{f1}$, and Stanton number St_{peak}/St_1 are shown in Fig. 11 with respect to the inviscid shock strength $\xi = p_2/p_1$. The skin-friction measurements from Ref. 8 are also included. In Fig. 11, the empirical correlations for the normalized pressure and the least-squares best fit to the skin-friction and heat transfer data are also shown as solid lines. The correlation for pressure is given as[12,25]

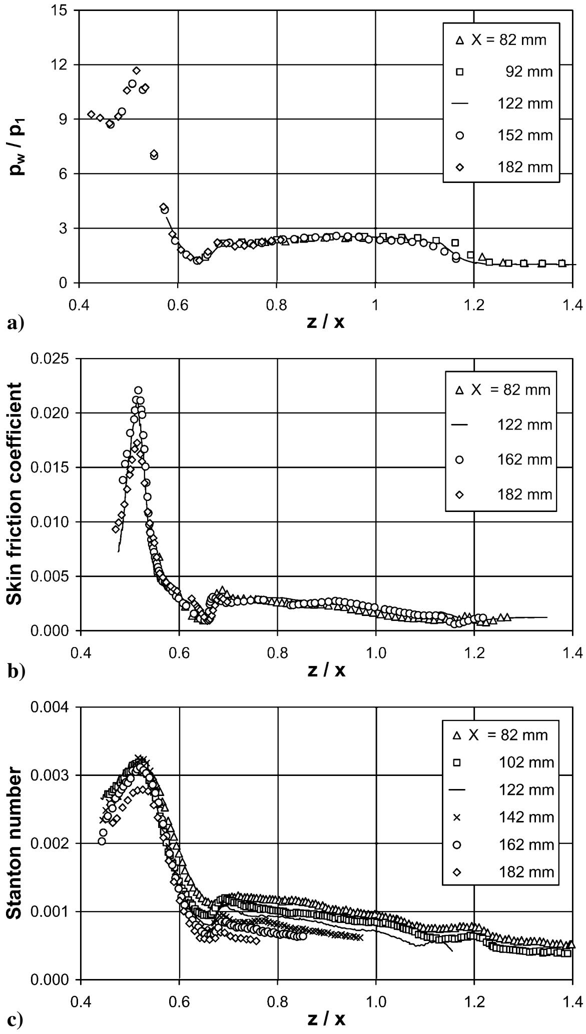

Fig. 10 Surface property results for 23-deg single fin at different *x* positions: a) pressure, b) skin-friction coefficient, and c) Stanton number.

$$p_{w\,\mathrm{peak}}/p_{w1} = 1.3\xi - 0.3\xi_i \tag{10}$$

where ξ_i is the critical shock strength at incipient three-dimensional separation, $\xi_i = 1.4$–1.6 (Ref. 11). The least-squares fit for the skin friction and Stanton number are

$$c_{f\,\mathrm{peak}}/c_{f1} = 0.9354\xi^{1.332} \tag{11}$$

$$St_{\mathrm{peak}}/St_1 = 1.1086\xi^{0.8992} \tag{12}$$

The comparison of these results shows that the surface parameters vary in a manner with respect to shock strength ξ. In particular, relative to the pressure growth, the Stanton number increases less rapidly as the shock strength is increased and the skin friction increases more rapidly. These different variations between the skin friction and heat transfer suggests that the relatively simple Reynolds analogy is of limited validity in strong three-dimensional SWTBLIs.

These results also indicate the limitations, in nonequilibrium flows, of indirect methods for skin-friction measurements.[3] These limitations arise due to the questionable use of similarity laws for the determination of skin friction when such measurements are based on the heat transfer processes, for example, when a buried wire sensor is used. The GISF technique, which is based on the principle

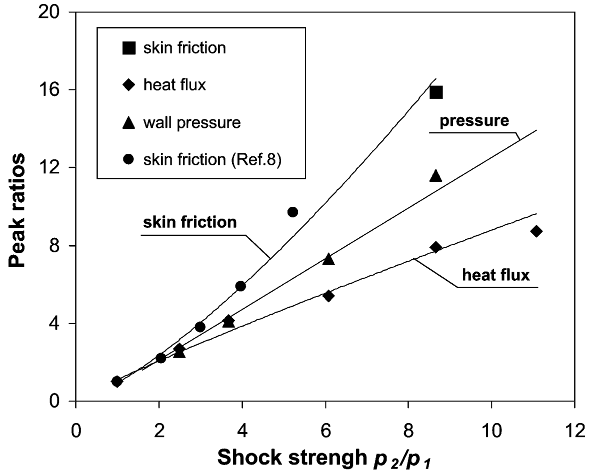

Fig. 11 Peaks ratios of skin friction, wall pressure, and Stanton number at primary attachment lines in vicinity of single fins vs inviscid shock strength.

of oil-film interferometry, and is used in the present work, does not have these limitations.

Conclusions

Two CFD validation cases for SWTBLI have been studied using modern nonintrusive methods for the measurement of skin friction and heat flux measurement. The two-dimensional case is the oblique shock interaction on a flat plate, and the three-dimensional case is the interaction of a swept shock generated by a single fin on a flat plate. In both test cases, a turbulent boundary layer developed in freestream of Mach number $M_\infty = 5$. The most significant findings of the study may be summarized as follows:

1) For the two-dimensional case, within the separated flow the skin friction decreases in the streamwise direction, whereas the heat flux increases. These different trends are indicative of the complex nonequilibrium behavior in the region of SWTBLI.

2) The surface pressure first reaches a constant value downstream of the two-dimensional shock reflection at the reattachment point; at this location the heat flux and skin friction are also maximum.

3) In the three-dimensional case, the skin friction and heat transfer are, in general, larger along the reattachment lines and lower along the separation lines. The locations of these lines are in good agreement with the locations of the peaks and valleys in the distributions of skin friction and heat transfer.

4) A local maximum in the skin-friction and heat transfer measurements is seen near the primary separation line S_1. These maxima are thought to be the result of an acceleration of the reversed flow, which occurs in the presence of a favorable pressure gradient. This mechanism of separation line suction should exist in some three-dimensional flows with open separation zones.

5) The skin-friction distribution along conical rays in the three-dimensional SWTBLI changes little in the downstream direction; on the other hand, there is a noticeable decrease in the heat flux.

6) The ratios of the normalized (that is, peak to undisturbed values) wall pressure, skin friction, and heat transfer show different behaviors with respect to the shock strength. Relative to the pressure, the Stanton number increases less rapidly and the skin friction more rapidly as the shock strength is increased.

7) The results of the present study suggest that the indirect methods of skin-friction measurements, which are based on similarity laws, such as the Reynolds analogy (for the heated film or buried wire techniques, for example) or the wall-wake law (for example, the velocity profile, Preston, or Stanton tube techniques), may be of limited utility in SWTBLI regions because the similarity laws break down. The technique based on the principle of oil-film interferometry does not suffer from these limitations.

Acknowledgments

The author thanks the partners from the Institute of Theoretical and Applied Mechanics, Russian Academy of Sciences at Novosibirsk: Alexander Zheltovodov for collaboration and many helpful discussions and Alexander Pavlov for many discussions on optical measurement techniques. He also acknowledges his colleagues from the DLR German Aerospace Center, Institute of Aerodynamics and Flow Technology: Henning Rosemann for helpful discussions and support of these activities, Anke Kovar for comments on the manuscript, and Lothar Budke and Karsten Pfeiffer from the Ludwieg Tube Wind Tunnel staff for their assistance in executing the experiments.

References

[1] Knight, D., Yan, H., Panaras, A. G., and Zheltovodov, A., "Advances in CFD Prediction of Shock Wave Turbulent Boundary Layer Interactions," *Progress in Aerospace Sciences*, Vol. 39, No. 2, 2003, pp. 121–184.

[2] Settles, G. S., and Dolling, D. S., "Swept Shock/Boundary-Layer Interactions—Tutorial and Update," AIAA Paper 90-0375, Jan. 1990.

[3] Settles, G. S., "Recent Skin Friction Technologies for Compressible Flows," AIAA Paper 86-1099, May 1986.

[4] Schülein, E., Krogmann, P., and Stanewsky, E., "Documentation of Two-Dimensional Impinging Shock/Turbulent Boundary Layer Interaction Flow," DLR, German Aerospace Center, Rept. IB 223-96 A 49, Göttingen, Germany, Oct. 1996.

[5] Fedorova, N. N., Fedorchenko, I. A., and Schülein, E., "Experimental and Numerical Study of Oblique Shock Wave/Turbulent Boundary Layer Interaction at $M = 5$," *Computational Fluid Dynamics Journal*, Vol. 10, No. 3, Special Issue, 2001, pp. 376–381.

[6] Lindblad, I., Wallin, S., Johanson, A., Friedrich, R., Lechner, R., Krogmann, P., Schülein, E., Courty, J., Ravachol, M., and Giordano, D., "Method for High Speed Turbulent Separated Flows with Experimental Verification," AIAA Paper 98-2547, June 1998.

[7] Steelant, J., "Effect of a Compressibility Correction on Different Turbulence Models," *Engineering Turbulence Modelling and Experiments 5*, edited by W. Rodi and N. Fueyo, Elsevier, 2002, pp. 207–216.

[8] Kim, K.-S., Lee, Y., Alvi, F. S., Settles, G. S., and Horstman, C. C., "Skin-Friction Measurements and Computational Comparison of Swept Shock/Boundary-Layer Interactions," *AIAA Journal*, Vol. 29, No. 10, 1991, pp. 1643–1650.

[9] Zheltovodov, A., Maksimov, A., Schülein, E., Knight, D., Thivet, F., Gaitonde, D., and Schmisseur, J., "Experimental and Computational Studies of Crossing-Shock-Wave/Turbulent Boundary-Layer Interactions," *Proceedings of the International Conference* "Recent Development in Applied Mathematics and Mechanics Theory, Experiment and Practice," *Computational Technologies*, Vol. 6, Pt. 2, edited by Y. I. Shokin, Inst. of Computational Technologies, Russian Academy of Sciences, Siberian Div., Novosibirsk, Russia, 2001, pp. 153–162.

[10] Alvi, F. S., and Settles, G. S., "Physical Model of the Swept Shock-Wave/Turbulent Boundary-Layer Interaction Flowfield," *AIAA Journal*, Vol. 30, No. 9, 1992, pp. 2252–2258.

[11] Zheltovodov, A., "Shock Waves/Turbulent Boundary Layer Interactions—Fundamental Studies and Applications," AIAA Paper 96-1977, June 1996.

[12] Zheltovodov, A., Maksimov, A., and Schülein, E., "Development of Turbulent Separated Flows in the Vicinity of Swept Shock Waves," *The Interactions of Complex 3-D Flows*, edited by A. M. Kharitonov, Inst. of Theoretical and Applied Mechanics, USSR Academy of Sciences, Novosibirsk, Russia, 1987, pp. 67–91.

[13] Ludwieg, H., Hottner, T., and Grauer-Carstensen, H., "Der Rohrwindkanal der Aerodynamischen Versuchsanstalt Göttingen," *Jahrbuch der DGLR 1969*, edited by H. Blenk and W. Schulz, DGLR, Cologne, Germany, 1970, pp. 52–58 (in German).

[14] Naughton, J. W., and Sheplak, M., "Modern Developments in Shear-stress Measurements," *Progress in Aerospace Sciences*, Vol. 38, No. 6, 2002, pp. 515–570.

[15] Tanner, L., and Blows, L., "A Study of the Motion of Oil Films on Surfaces in Air Flow, with Application to the Measurement of Skin Friction," *Journal of Physics, E: Scientific Instruments*, Vol. 9, No. 3, 1976, pp. 194–202.

[16] Schülein, E., "Development and Application of the Thin Oil Film Technique for Skin Friction Measurements in the Short-Duration Hypersonic Wind Tunnel," *New Results in Numerical and Experimental Fluid Mechanics IV*, edited by C. Breitsamter, B. Laschka, and H.-J. Heinemann, Vol. 87, Notes on Numerical Fluid Mechanics and Multidisciplinary Design, Springer, Berlin, 2004, pp. 407–414.

[17]Maksimov, A. I., Pavlov, A. A., and Shevchenko, A. M., "Development of the Optical Skin Friction Measurement Technique for Supersonic Gradient Flows," *Proceedings of the International Conference on the Methods of Aerophysical Research*, Pt. 2, Inst. of Theoretical and Applied Mechanics, Russian Academy of Sciences, Siberian Div., Novosibirsk, Russia, 1994, pp. 172–177.

[18]Pavlov, A. A., "Development of Panoramic Optical Diagnostics Methods for 3-D Flows," Ph.D. Dissertation, Inst. of Theoretical and Applied Mechanics, Russian Academy of Sciences, Siberian Div., Novosibirsk, Russia, June 1995 (in Russian).

[19]Schlichting, H., *Boundary Layer Theory*, 6th. ed., McGraw–Hill, New York, 1968, p. 312.

[20]Schülein, E., Koch, S., and Rosemann, H., "Skin Friction Measurement and Transition Detection Techniques for the Ludwieg-Tubes at DLR," *Advanced Aerodynamic Measurement Technology*, CP-601, AGARD, 1998, pp. 23-1–23-9.

[21]Schülein, E., "Optical Skin Friction Measurements in the Short-Duration Ludwieg Tube Facility," *ICIASF 2003 Record: Proceedings of the 20th International Congress on Instrumentation in Aerospace Simulation Facilities*, Inst. of Electrical and Electronics Engineers, 2003, pp. 157–168.

[22]Schultz, D. L., and Jones, T. V., "Heat-Transfer Measurements in Short-duration Hypersonic Facilities," AGARDograph-165, AGARD, Feb. 1973.

[23]Krogmann, P., and Schwane, R., "Synthesis of TC T1-97: Hyperboloid-Flare at RWG Conditions," *Proceedings of the First Europe–US High Speed Flow Field Database Workshop*, Pt. 2, edited by S. Borrelli, M. Marini, F. Grasso, and J. Periaux, Italian Aerospace Research Center, Capua, Italy, 1997, pp. 127–136.

[24]Fedorova, N. N., and Fedorchenko, I. A., "Computations of Interaction of an Incident Oblique Shock Wave with a Turbulent Boundary Layer at a Flat Plate," *Journal of Applied Mechanics and Technical Physics*, Vol. 45, No. 3, 2004, pp. 358–366.

[25]Schülein, E., and Zheltovodov, A. A., "Documentation of Experimental Data for Hypersonic 3-D Shock Waves/Turbulent Boundary Layer Interaction Flows," DLR, German Aerospace Center, Rept. IB 223-99 A 26, Göttingen, Germany, March 2001.

N. Chokani
Associate Editor